A Kinetic Energy Analysis of a Microburst-Producing Thunderstorm Based on JAWS Dual-Doppler Data

YEONG-JER LIN AND JOHN A. COOVER

Department of Earth and Atmospheric Sciences, Saint Louis University, Saint Louis, Missouri

(Manuscript received 26 October 1987, in final form 7 April 1988)

ABSTRACT

Dual-Doppler data collected from 1646 to 1648 MDT 14 July 1982 in Colorado are used to study the kinetic energy budget of a microburst-producing thunderstorm during its mature stage. Values of each term in the kinetic energy budget equation are assessed from the Doppler derived winds and retrieved thermodynamic fields using a fourth-order finite differencing with 0.5 km grid spacing. Results indicate that vertical totals of the horizontal generation and horizontal flux divergence terms act as a source of kinetic energy, while a vertical total of dissipation is a sink. The horizontal flux divergence term is nearly in balance with the vertical flux divergence term. Similarly, the vertical generation and total buoyancy production terms have the same order of magnitude but opposite signs at most levels. In the lower layer, where the microburst dominates, the kinetic energy is transported downward. In the middle and upper layers, the kinetic energy is transported upward due to the storm's strong convective updrafts.

1. Introduction

There are very few observational studies in the literature that describe the effects of areas of intense convection on their mesoscale environments. Most mesoscale, diagnostic kinetic energy studies have examined how large areas of convection can modify the larger synoptic-scale kinetic energy balance. Using rawinsonde data from the National Severe Storms Laboratory (NSSL), Kung and Tsui (1975) and Tsui and Kung (1977) studied the meso β-scale storm environment. Findings showed that environments containing intense convection are characterized by large generation and dissipation of kinetic energy at the jet stream level. Conversely, nonconvective environments exhibit dissipation of kinetic energy from subgrid to grid scales of motion. Using the data collected from the Atmospheric Variability Experiment and Severe Environmental Storms and Mesoscale Experiment (AVESESAME) projects, Fuelberg and Jedlovec (1982) and Fuelberg and Printy (1984) conducted meso α- and meso β-scale kinetic energy studies, respectively. Results showed that the convective environment was energetically very active when compared to the entire analyzed domain. Magnitudes of energy transformations in the convective environment are significantly larger and their effects are more discernible than at the synoptic scale.

Today, dual- and multiple-Doppler radar measurements can provide a detailed wind field within a convective storm. With the aid of thermodynamic retrieval techniques (e.g., Gal-Chen 1978; etc.), pressure and buoyancy fields inside the storm can be retrieved from the derived three-dimensional wind field (Hane and Ray 1985; Lin et al. 1986; etc.). A study of the kinetic energy budget of a convective storm using the Doppler derived winds and the retrieved pressure and buoyancy fields may reveal some important physical processes maintaining the storm structure.

Kinematic, dynamic and thermodynamic properties of a microburst-producing storm were studied by Lin and Hughes (1987) and Lin et al. (1987) using dual-Doppler data. This storm occurred on 14 July 1982 within the network of Joint Airport Weather Studies (JAWS) in Denver, Colorado.

The present study is an extension of the studies by Lin and Hughes (1987) and Lin et al. (1987) employing the same dataset. The purpose is to investigate the kinetic energy budget of a microburst-producing storm during the storm's mature stage. Budgets are assessed over the domain of 10 km × 10 km (centered on the microburst) at each analysis level. The important physical processes contributing to the kinetic energy budget are studied. The goal is to better understand the structure and internal dynamics of the storm which produced a microburst at low levels.

2. Data and computational procedures

The data analysis and reduction procedures were detailed in studies by Lin et al. (1987) and Lin and

Corresponding author address: Dr. Yeong-jer Lin, Dept. of Earth and Atmospheric Sciences, Saint Louis University, P.O. Box 8099-Laclede Station, Saint Louis, MO 63156.

Hughes (1987). Dual-Doppler data observed from 1646 through 1648 MDT were judiciously analyzed to produce a detailed wind field. There were 19 analysis levels ranging from 0.25 km to the storm top at 8.5 km. The horizontal grid spacing was 0.5 km, while the vertical grid spacing varied from 0.25 km for levels below 1 km to 0.5 km for those above 1 km. Vertical velocities were computed from the anelastic continuity equation by integrating downward from the storm top with variational adjustment.

The analysis equations employed to adjust the u and v components were

$$u - u^o = \frac{\bar{\rho}}{2\alpha^2}\frac{\partial \lambda}{\partial x} \tag{1}$$

$$v - v^o = \frac{\bar{\rho}}{2\beta^2}\frac{\partial \lambda}{\partial y} \tag{2}$$

$$\int_{z_t}^{0} \nabla_3 \cdot \bar{\rho} v \, dz = 0 \tag{3}$$

where the overbar denotes a mean (environmental) quantity, the superscript o represents an observed quantity, α^2 and β^2 are two weighting factors which were related to the variances of the u- and v-component uncertainty, respectively, and λ is the Lagrange multiplier. Equations (1) and (2) are Euler–Lagrange equations of the variational formalism and (3) is the constraint equation. With the aid of (1) and (2) and the anelastic continuity equation applied to the vertically integrated horizontal mass divergence as an integral constraint, we arrived at

$$\int_{z_t}^{0} \bar{\rho}\left[\frac{\partial}{\partial x}\left(\frac{\bar{\rho}}{2\alpha^2}\frac{\partial \lambda}{\partial x}\right) + \frac{\partial}{\partial y}\left(\frac{\bar{\rho}}{2\beta^2}\frac{\partial \lambda}{\partial y}\right)\right] dz = (\bar{\rho} w^o)_{\text{sfc}}. \tag{4}$$

This equation was solved via successive overrelaxation (SOR). Subsequently, the horizontal components of true winds (u, v) were determined from (1) and (2) in which the volume means were used to represent the weighting factors. Finally, the true w field at any level z_1, was calculated from the formula

$$w_1 = w_1{}^o - \frac{(\bar{\rho} w^o)_{\text{sfc}}}{\bar{\rho}_1}\left[\frac{\int_{z_t}^{z_1} \bar{\rho}\, dz}{\int_{z_t}^{0} \bar{\rho}\, dz}\right]. \tag{5}$$

The derived wind field is subject to both random and nonrandom errors. Using the technique similar to that of Wilson et al. (1984), an error analysis was conducted. Our finding shows that the combined errors due to statistical uncertainty in the radial velocity estimates and geometrical considerations are approximately 1–2 m s^{-1} for the horizontal derived winds. The error in vertical velocity is more difficult to estimate since it includes both nonrandom and random errors. However, our efforts in data reduction and application of variational adjustment to the three Cartesian wind components (u, v, w) have reduced the errors considerably (Lin et al. 1986; Lin and Hughes 1987).

Once the detailed wind field was derived, fields of deviation perturbation pressure and virtual temperature were recovered from the derived three-dimensional wind field via a thermodynamic retrieval method (Gal-Chen 1978). For detail, see studies by Lin et al. (1987) and Lin and Hughes (1987). The retrieved fields were subjected to momentum checks (E_r) (see Eq. (19) in Lin et al. 1986) to determine the level of confidence before interpretation. Values of E_r represent relative errors in pressure retrieval. Such values are used to find out how well the derived pressure perturbations balance the dynamic equations. Smaller values of E_r (<0.5) are desirable; however, Hane and Ray (1985) pointed out that fields which contain much relevant information can also produce large E_r values in the neighborhood of 1. Thus, E_r should only be considered as a relative measure of goodness of fit of the perturbation pressure gradients, and the acceleration and friction terms in the horizontal momentum equations. It is equally important to examine the physical consistency of thermodynamic perturbations with respect to the storm's kinematic structure at the analysis time. For example, the retrieved fields must be in overall agreement with the fields of vertical velocity, convergence/divergence and vorticity.

Only one volume scan from 1646 to 1648 MDT was considered in studies by Lin and Hughes (1987) and Lin et al. (1987); therefore, local time tendencies in the dynamic equations cannot be evaluated. For an ordinary, transient thunderstorm, such as the microburst-producing storm being investigated, the quasi-steady state assumption is questionable. Omission of the tendency terms in the dynamic equations will result in errors to the pressure and buoyancy retrievals (Hane et al. 1981). Our calculation revealed that the standard deviation of the advective terms in the horizontal momentum equations is about 0.01 m s^{-2} (see Table 1 in Lin et al. 1987). This magnitude is comparable to a local time rate of change of 3 m s^{-1} in 5 min. Hence, local time changes on this order, which could easily occur in microbursts (Wilson et al. 1984), are likely to significantly affect the pressure and temperature retrievals. For this reason, caution must be exercised in interpreting the pressure and temperature fields. The momentum checks (E_r) obtained by Lin and Hughes (1987; see their Fig. 5) showed relatively small values ($E_r < 0.2$) in the lowest layer below 1 km with relatively large values aloft. The mean value of E_r for the entire storm is about 0.4. It is possible that the quasi-steady state assumption may have contributed in part to the larger values of E_r. An additional study is needed in order to determine the effect of local time change on the pressure retrieval using dual-Doppler data collected from three successive deep volume scans. Simulation

studies by Gal-Chen (1978) and Hane et al. (1981) showed that the only way to reduce the temporal evolution error is to scan the storm more rapidly so that the local time tendencies can be more accurately computed.

3. Kinetic energy equation

The momentum equations in a Cartesian coordinate system can be written as

$$\frac{\partial u}{\partial t} = -u\frac{\partial u}{\partial x} - v\frac{\partial u}{\partial y} - w\frac{\partial u}{\partial z} - \frac{1}{\bar{\rho}}\frac{\partial P'}{\partial x} + F_x \quad (6)$$

$$\frac{\partial v}{\partial t} = -u\frac{\partial v}{\partial x} - v\frac{\partial v}{\partial y} - w\frac{\partial v}{\partial z} - \frac{1}{\bar{\rho}}\frac{\partial P'}{\partial y} + F_y \quad (7)$$

$$\frac{\partial w}{\partial t} = -u\frac{\partial w}{\partial x} - v\frac{\partial w}{\partial y} - w\frac{\partial w}{\partial z} - \frac{1}{\bar{\rho}}\frac{\partial P'}{\partial z} + g\left(\frac{T'_v}{\bar{T}_v} - q_l\right) + F_z \quad (8)$$

where a prime represents the deviation from the environmental mean, and other symbols have their conventional meanings. Note that the Coriolis terms are excluded in (6)–(8) since they are found from scale analysis to be much smaller than the other terms.

In the preceding equations, the frictional term, **F**, was formulated based on the parameterization of Klemp and Wilhelmson (1978) discussed in detail in Lin et al. (1987). The liquid water mixing ratio, q_l, was approximated by the rainwater mixing ratio (q_r). Values of q_r were empirically estimated from radar reflectivity, i.e.,

$$q_r = \frac{1}{\bar{\rho}}\left\{\frac{Z\,(\text{mm}^6\,\text{m}^{-3})}{A}\right\}^{1/B}, \quad (9)$$

where $A = 1.73 \times 10^4$ and $B = 7/4$ (Kessler 1969). The assumption of water loading in (8) which can be measured by the radar is only valid below cloud base and will contain the largest error within the updraft.

Multiplying u, v and w on (6)–(8), respectively, adding, noting that $\nabla\cdot\bar{\rho}\mathbf{v} = 0$ and averaging over the 10 km × 10 km horizontal domain, we arrived at the following kinetic energy equation for a nonhydrostatic system:

$$\underbrace{\left\langle\frac{\partial\bar{\rho}K_3}{\partial t}\right\rangle}_{\text{LTK}} = \underbrace{-\langle\nabla_h\cdot(\bar{\rho}K_3\mathbf{V}_h)\rangle}_{\text{HFD}} - \underbrace{\left\langle\frac{\partial\bar{\rho}K_3w}{\partial z}\right\rangle}_{\text{VFD}} - \underbrace{\langle\mathbf{V}_h\cdot\nabla_hP'\rangle}_{\text{HGE}} - \underbrace{\left\langle w\frac{\partial P'}{\partial z}\right\rangle}_{\text{VGE}} + \underbrace{\left\langle\bar{\rho}gw\left(\frac{T'_v}{\bar{T}_v} - q_l\right)\right\rangle}_{\text{BUP}} + \underbrace{\langle\bar{\rho}\mathbf{V}\cdot\mathbf{F}\rangle}_{\text{FDI}} \quad (10)$$

where $\langle(\ \ )\rangle \equiv (1/\text{Area})\iint(\ \ )dxdy$, $K_3 = (u^2 + v^2 + w^2)/2$ is the total kinetic energy per unit mass, and other symbols have their usual meanings. Terms on the right-hand side of (10) represent the horizontal flux divergence (HFD), the vertical flux divergence (VFD), the horizontal generation (HGE), the vertical generation (VGE), the total buoyancy production (BUP) and the dissipation (FDI) of kinetic energy, respectively.

As noted earlier, the thermodynamic retrieval method of Gal-Chen (1978) was employed to retrieve pressure and temperature perturbations from the derived wind field. This method recovered fields of deviation perturbation pressure and virtual temperature (P'_d and T'_{vd}) defined as

$$\left.\begin{aligned} P'_d &\equiv P' - \langle P'\rangle \\ T'_{vd} &\equiv T'_v - \langle T'_v\rangle \end{aligned}\right\}. \quad (11)$$

Here P' is the pressure perturbation from the environmental mean ($\bar{P}$) and T'_v is the virtual temperature perturbation from the environmental mean ($\bar{T}_v$).

With the aid of (11), the vertical generation term (VGE) can be approximated by

$$-\left\langle w\frac{\partial}{\partial z}(P'_d + \langle P'\rangle)\right\rangle = -\left\langle w\frac{\partial P'_d}{\partial z}\right\rangle - \langle w\rangle\frac{\partial\langle P'\rangle}{\partial z} \approx -\left\langle w\frac{\partial P'_d}{\partial z}\right\rangle. \quad (12)$$

Similarly, the thermal buoyancy term in term BUP can be approximated by

$$\left\langle\frac{\bar{\rho}gw}{\bar{T}_v}(T'_{vd} + \langle T'_v\rangle)\right\rangle = \frac{\bar{\rho}g}{\bar{T}_v}(\langle wT'_{vd}\rangle + \langle w\rangle\langle T'_v\rangle) \approx \frac{\bar{\rho}g}{\bar{T}_v}\langle wT'_{vd}\rangle. \quad (13)$$

Since the unknown area means, $\partial\langle P'\rangle/\partial z$ and $\langle T'_v\rangle$, are nonzero (which vary with height), the validity of (12) and (13) depends upon the area-mean $\langle w\rangle$ going to zero or remaining very small. For a typical convective storm with updrafts and downdrafts in coexistence, the $\langle w\rangle$ value averaged over the whole horizontal domain, in general, will be much smaller than magnitudes of the updrafts and downdrafts at a given height. Our calculation shows that $\langle w\rangle$ has small negative values at levels below 3 km with positive values aloft (Table 1). Magnitudes of $\langle w\rangle$ range from −0.3 to 1.2 m s^{-1}. For comparison, maximum updraft and downdraft speeds ($w_{\max}$) for updrafts UP1 and UP2 and downdrafts DN1 and DN2 at each level are also shown in Table 1. Among these, DN1 produced the microburst at low levels. Inspection of Table 1 reveals that values of $\langle w\rangle$ are one order of magnitude smaller than $w_{\max}$ at most levels except in the layer between 5 and 8 km. Negative values of $\langle w\rangle$ in the lower layer are attributed to the dominance of downdrafts in that layer. Conversely, positive values prevail in the middle

TABLE 1. Values of maximum updraft and downdraft speeds (w_{max}) and the area mean $\langle w \rangle$ at each height. Here UP1 and UP2 signify updrafts, while DN1 and DN2 denote downdrafts. Units are in meters per second.

Z (km)	$\langle w \rangle$ (m s^{-1})	w_{max} (m s^{-1})			
		UP1	UP2	DN1	DN2
8.5	0	0	0	0	0
8.0	0.4	1	1	1	0
7.5	0.8	2	1	1	−1
7.0	1.0	4	2	0	−2
6.5	1.1	5	3	0	−3
6.0	1.2	6	5	−1	−4
5.5	1.2	6	7	−2	−4
5.0	1.1	7	8	−3	−5
4.5	0.9	6	9	−4	−6
4.0	0.6	6	8	−5	−7
3.5	0.3	5	7	−6	−8
3.0	0.1	5	7	−7	−7
2.5	−0.1	4	6	−8	−7
2.0	−0.2	4	5	−9	−6
1.5	−0.2	4	4	−8	−5
1.0	−0.3	3	3	−7	−4
0.75	−0.3	3	2	−6	−3
0.50	−0.2	2	2	−5	−2
0.25	−0.1	1	1	−3	−1

and upper layers, since updrafts are stronger than downdrafts in those layers. Although the magnitude of $\langle w \rangle$ is much smaller than that of w_{max} at every level, it is not nearly zero unless dual-Doppler measurements are taken over a domain which is far larger than that considered in this study. For this reason, caution must be exercised in interpreting terms VGE and BUP, since both terms contain an unknown horizontal average that is not represented in (12) and (13). Nevertheless, findings presented in Table 1 suggest that the approximations (12) and (13) appear to be justified especially in the layer below 4 km where $\langle w \rangle$ is very small.

4. Discussion of results

Budgets of the total kinetic energy, per unit volume, were calculated from (10), over the 10 km × 10 km horizontal domain centered on the microburst. At the time of analysis, the microburst was located at 12.5 km west and 18 km south of the CP-2 radar (Fig. 1).

Figure 2 displays vertical variations of terms HFD and VFD. Our sign convention is positive (negative) for convergence (divergence). Note that term HFD has positive values at levels between 1–6 km with negative values aloft, in agreement with the field of horizontal convergence/divergence (not shown). Near the surface, there is a small negative value (divergence) associated with the microburst-diverging outflow in that layer. Conversely, the contribution from term VFD gives flux divergence of kinetic energy in the lower and middle layers with flux convergence in the upper layer. In the lowest layer ($z < 1$ km) where the microburst dominates, there is vertical flux convergence of kinetic energy. Inspection of Fig. 2 reveals that terms HFD and VFD have the same order of magnitude but op-

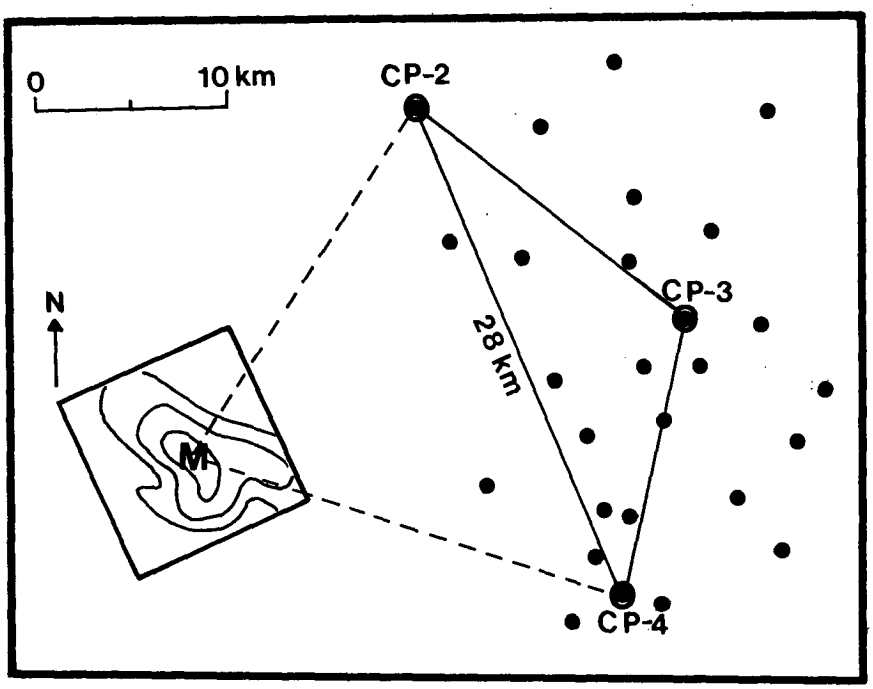

FIG. 1. Locations of three NCAR radars and 27 PAM stations (solid dot). The box represents the 10 km × 10 km horizontal domain for the kinetic energy budget calculation. The microburst center is signified by a symbol M.

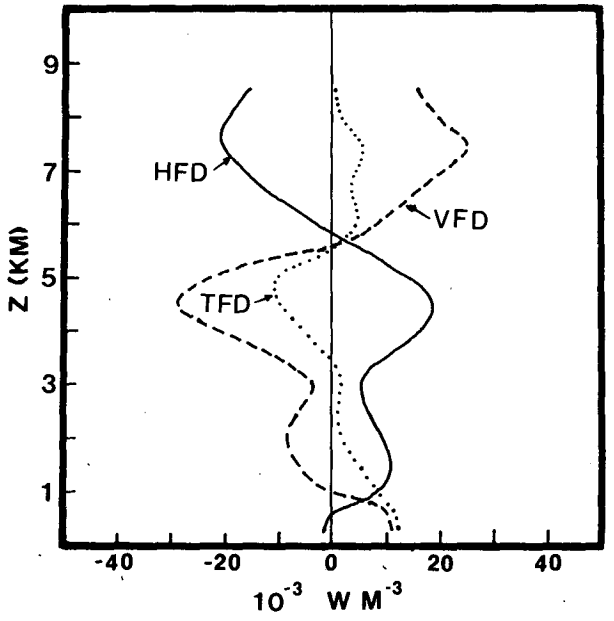

FIG. 2. Vertical variations of the horizontal flux divergence (HFD), vertical flux divergence (VFD) and total flux divergence (TFD) of kinetic energy. Units are in 10^{-3} W m^{-3}.

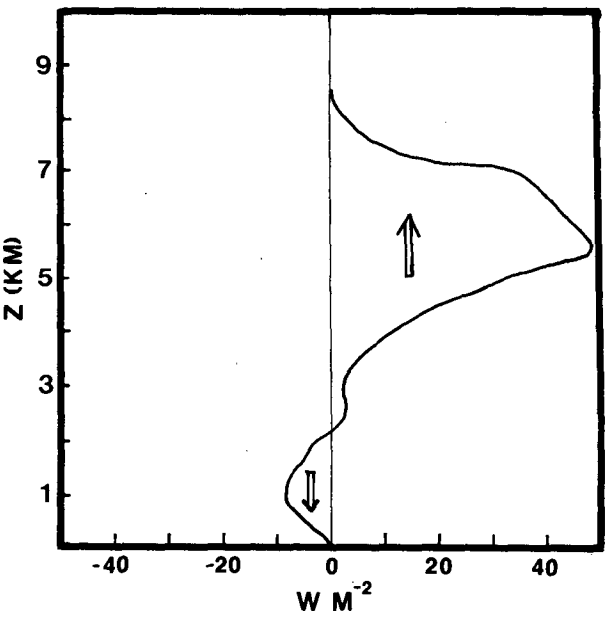

FIG. 3. The vertical distribution of mean vertical kinetic energy transport $\langle \bar{\rho} K_3 w \rangle$.

posite sign at most levels. The sum of these two terms represents the total flux divergence of kinetic energy (TFD), which is also plotted in Fig. 2 (dotted line). The interplay between HFD and VFD results in a net loss of kinetic energy in the middle troposphere from 3.5 to 5.5 km and a net gain in the lower and upper troposphere. The largest gain, found in the lowest layer ($z < 1$ km), is of particular significance since it is closely related to the microburst occurrence in that layer. The vertical transport of kinetic energy, $\langle \bar{\rho} K_3 w \rangle$, is depicted in Fig. 3. This quantity shows how the total kinetic energy is transferred from one layer to another. In the lower layer, the kinetic energy is transported downward as a result of the organized downdraft associated with the microburst at low levels. In the middle and upper layers ($z > 2$ km), the kinetic energy is transported upward to maintain the storm's convective activity.

The contributions from terms HGE and VGE to the kinetic energy change are shown in Fig. 4. Notice that the horizontal generation term (HGE) provides a source of kinetic energy at levels below 4.5 km with a sink above. The positive contribution of HGE occurs when the wind blows from high pressure to low pressure in the horizontal direction. As found in the study by Lin and Hughes (1987) (see their Fig. 10), a strongly horizontal diverging outflow from the microburst center is accompanied by a pronounced horizontal perturbation pressure gradient at low levels, resulting in a positive contribution of HGE. In the middle troposphere, the presence of high pressure on the upshear side of the updraft (U) with low pressure on the downshear side also produces positive values of HGE up to 4.5 km. On the other hand, the contribution from term VGE is positive at low levels ($z < 1$ km) in conjunction with the microburst occurrence. Negative values occur in the layer from 1 to 4.5 km, where vertical velocity is negatively correlated with vertical pressure gradient

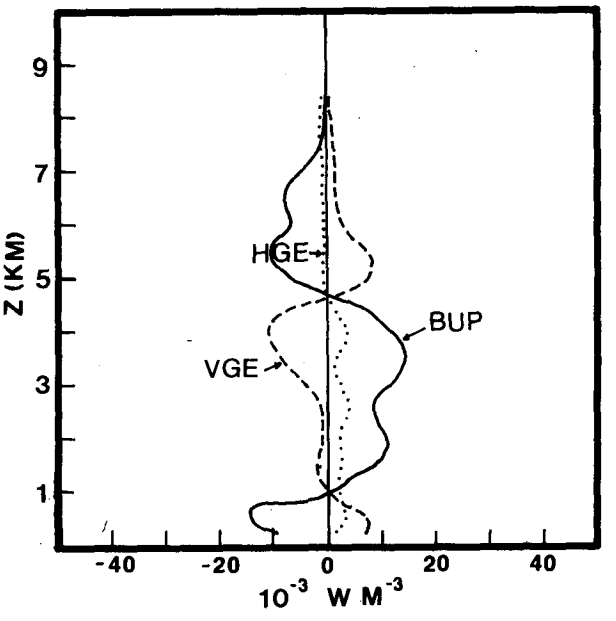

FIG. 4. As in Fig. 2 except for the horizontal generation (HGE), vertical generation (VGE) and total buoyancy production (BUP) of kinetic energy.

$(-\partial P'/\partial z)$. Conversely, vertical velocity is positively correlated with vertical pressure gradient in the layer above 4.5 km, resulting in positive values of VGE.

In Fig. 4, the kinetic energy production due to the total buoyancy (BUP) is also plotted (solid line). This term consists of the contributions of thermal buoyancy and precipitation loading. It is of great importance in a convective storm such as the one under study due to the presence of heavy precipitation and vigorous vertical motion. A source of kinetic energy from the buoyancy production occurs when the warm air rises and the cold air descends, while a sink develops when the warm air is forced to descend and the cold air is lifted upward.

As explained in Lin and Hughes (1987), the air in the microburst core is warmer than the environment. This finding is consistent with those reported in studies by Fujita (1985) and Srivastava (1985). Based on the temperature observations taken at the PAM stations during JAWS, Fujita (1985) found that the air temperature in a microburst can be either warmer or colder than its environment. In a wet microburst with a strong downflow, the air temperature is likely to be warmer than its surrounding. He explained that downflow air can warm up dry-adiabatically all the way to the ground, unless embedded raindrops can evaporate fast enough to maintain a moist-adiabatic descent.

Unlike Fujita's observational study, Srivastava (1985) employed a simple numerical model to investigate the evaporatively driven downdraft associated with a high-based cumulus similar to that observed in Colorado. He showed that the evaporation of raindrops cools the air, while the descending motion warms it (see his Fig. 1). However, in the region of the downdraft column of high relative humidity and strong downward air motion, the compressional warming due to descent dominates, resulting in the temperature excess within the downdraft. Conversely, the temperature deficit develops in the region with low relative humidity and weak downward air speed. The maximum cooling occurs at the level where the vertical velocity is reduced to practically zero.

Inspection of Fig. 4 reveals that values of BUP are negative in the lowest layer ($z < 1$ km) where the microburst dominates. In this layer, the downdraft carries the warmer air, resulting in a sink of kinetic energy at levels below 1 km. In the subcloud layer from 1 to 3.5 km, downward motion and evaporative cooling prevail, producing a source of kinetic energy by cold air sinking in that layer. In the middle layer above the cloud base (3.5–4.5 km), the warm air ascends within the updrafts, due to latent heat releases by condensation, resulting in a gain of kinetic energy over that layer. Conversely, a sink of kinetic energy occurs in the upper layer ($z > 4.5$ km) where the cold air is lifted by the updrafts and the warm air is forced to descend by the downdrafts. Examination of Fig. 4 further reveals that terms VGE and BUP have the same order of magnitude but opposite sign at most levels. This result is consistent with the retrieved fields of P'_d and T'_{vd}. As explained in Lin and Hughes (1987) (see their Eq. (10)), the combined contributions due to precipitation loading and friction to the magnitude of temperature deviation (T'_{vd}) are one order of magnitude smaller than that of the vertical acceleration and vertical pressure gradient terms. Consequently, the vertical acceleration, vertical perturbation pressure gradient and buoyancy terms are nearly in balance. Among these, the vertical pressure gradient and the buoyancy generally have the same order of magnitude but opposite contributions to the net vertical acceleration. As a result, the vertical acceleration term in most areas is one order of magnitude smaller than that of the vertical pressure gradient and buoyancy terms.

It must be pointed out that the result presented in Fig. 4 is less accurate than that shown in Fig. 2. As depicted in (12) and (13), both VGE and BUP terms have an unknown horizontal average that is not represented. In addition, errors in thermodynamic retrieval could be significant due to the omission of local time tendencies in pressure and temperature computation (see section 2). For these reasons, the result shown in Fig. 4 should be carefully interpreted in a qualitative manner.

In the previous studies of kinetic energy balance, e.g., Tsui and Kung (1977), Fuelberg and Printy (1984), etc., emphasis was placed on the storm's environment using the conventional upper air data. In these studies, the dissipation term was not calculated directly. Instead, it was estimated from the kinetic energy budget equation as a residual. Therefore, the term contains a quantitative measure of the relevant physical processes plus the errors in computation of each of the terms in the budget equation. Unlike the previous energetic studies, the present study employs the Doppler derived winds within a convective system. These data provide fine spatial resolution with the horizontal grid spacing of 0.5 km. For this reason, an attempt is made to calculate the dissipation term (FDI) directly using the Klemp–Wilhelmson type parameterization mentioned previously. Lin et al. (1987) employed the same parameterization scheme to assess values of eddy viscosity and eddy stresses in the subcloud layer of the same storm and obtained good results.

Table 2 presents budgets of the total kinetic energy averaged over the 10 km × 10 km horizontal domain and integrated over a depth of 1 km. Units are in watts per unit area (W m^{-2}). Notice that term FDI has negative values (sink) at all layers. The magnitude is generally smaller than the other terms in the budget equation in each layer, which agrees with scale analysis. The bottom row in Table 2 presents the total budget of each term from the surface to the storm top at 8.5 km. Note that the dissipation term acts as a sink (−14 W m^{-2}) of kinetic energy, while the horizontal flux divergence term (10 W m^{-2}) and the horizontal gen-

TABLE 2. Kinetic energy budgets, averaged over the 10 km × 10 km horizontal domain and integrated over a depth of 1 km, at 1647 MDT 14 July 1982. Units are in W m^{-2}. The definition of each term is given in the text.

Layer (km)	HFD	VFD	HGE	VGE	BUP	FDI	LTK
7–top	−28.43	31.65	−0.49	0.23	−2.57	−1.38	−0.99
6–7	−10.43	14.70	−1.22	0.42	−7.40	−1.80	−5.73
5–6	4.86	−6.74	−1.23	6.10	−8.95	−2.68	−8.64
4–5	16.49	−26.03	0.61	−4.46	4.04	−1.81	−11.16
3–4	10.78	−12.30	1.88	−7.70	12.83	−1.35	4.14
2–3	6.37	−5.87	2.55	−2.01	9.22	−1.45	8.81
1–2	10.17	−5.39	1.74	−1.73	6.98	−1.62	10.15
Sfc–1	0.38	10.05	1.21	3.69	−8.12	−1.44	5.77
Vertical total	10.19	0.07	5.05	−5.46	6.03	−13.53	2.35

eration term (5 W m^{-2}) provide a source. Another source of kinetic energy (6 W m^{-2}) comes from the total buoyancy production term (BUP). The gain is nearly in balance with the loss due to term VGE (−6 W m^{-2}). The last column of Table 2 shows the local time change (LTK). This term is obtained from the sum of all terms on the right-hand side of (10); it is not determined from the observed dual-Doppler winds. As a consequence, the term is less reliable than each of the other terms in the budget equation. It contains not only the information of physical processes contributing to a gain/loss of kinetic energy, but also the errors in computation. These errors include the uncertainty in u, v, w, P'_d and T'_{vd} estimates, the parameterization errors in friction and precipitation loading, the truncation error, etc. The latter error is considerably reduced due to the utilization of fourth-order finite differencing and 0.5 km grid spacing. For these reasons, term LTK should be carefully interpreted in a qualitative manner. Notice that LTK has positive values at levels below 4 km with negative values aloft, indicating a net gain of kinetic energy in the lower troposphere and a net loss in the middle and upper troposphere. The integrated value over the whole storm volume is 2 W m^{-2}. This finding suggests that the kinetic energy of the lower levels is growing due to the microburst occurrence, while the upper levels of the storm are losing kinetic energy. As cautioned earlier, the result should be interpreted with care because of uncertainties in the estimates of LTK.

Findings presented in Figs. 2 and 4 and Table 2 pertain to a meso γ-scale convective storm in a nonhydrostatic system. The storm is an ordinary, nonsevere thunderstorm which produced the microburst at low levels. It is interesting to make some comparisons between our results for the storm itself and those of the storm environment. As depicted in section 1, several energetic studies of the mesoscale storm environment were reported in the literature; for example, see studies by Tsui and Kung (1977) and Fuelberg and Printy (1984). These studies utilized rawinsonde data collected in Oklahoma to investigate kinetic energy budgets of the meso β-scale storm environment using a pressure coordinate system. Because of the differences in geographical location, storm severity, etc., a quantitative comparison between our results and theirs is not practical. However, some qualitative discussion about similarities and differences would be of interest. In the study by Fuelberg and Printy (1984), the rawinsonde data at 75 km spacing and 3 or 1.5 h intervals were employed to analyze kinetic energy budgets of the near storm environment. The composite area–time averaged budget, based on the ten observation times, was given in their Table 1. Results showed that cross-contour flow provided the main source of kinetic energy with horizontal flux divergence and dissipation to unresolvable motion as the major sinks. The largest contributions of these terms occurred in the layer above 400 mb near the jet stream level. Note that the confidence level of rawinsonde measurements in the upper layer was much lower than that in the lower and middle layers. A cross-comparison between our results (Table 2) and theirs shows that magnitudes of the horizontal and vertical flux divergence terms for the storm scale is one order of magnitude greater than those for the storm environment in the lower and middle layers, while in the upper layer, both the storm itself and the environment have the same order of magnitude and similar sign. This feature demonstrates that the horizontal and vertical flux divergence terms play an important role in the kinetic energy balance of a convective storm in the lower and middle layers as compared to those in the storm environment. On the other hand, magnitudes of our generation terms (HGE and VGE) are about the same as those for the environment in the lower and middle layers, while in the upper layer the environment has much larger values than those in the storm itself. Notice that the method used to compute generation is quite different between the two studies. In regard to dissipation, our values are quite comparable with theirs at most levels, except in the upper layer. As mentioned previously, our study employed the parameterization of friction to estimate the dissipation term, whereas Fuelberg and Printy estimated dissipation from the kinetic energy equation as a residual. Consequently, their dissipation term was nearly

balanced by the horizontal generation term, having the same order of magnitude but opposite sign at most levels.

5. Conclusions

The Doppler derived winds and the retrieved thermodynamic variables were used to study the kinetic energy balance of a microburst-producing thunderstorm during its mature stage. Results show that 1) the kinetic energy is transferred downward near the surface as a result of the organized downdraft in the microburst area, while the kinetic energy is transported upward in the middle and upper layers due to the updrafts within the storm; 2) the horizontal flux divergence and horizontal generation terms act as a source of kinetic energy with dissipation as a sink; 3) the horizontal flux divergence of kinetic energy prevails in the upper layer, while the horizontal flux convergence dominates in the lower and middle layers. The horizontal and vertical flux divergence terms are nearly in balance, having the same order of magnitude but opposite sign; and 4) the total buoyancy production term is approximately balanced by the vertical generation term.

In the preceding conclusions, the last one should be interpreted with care. It is less reliable than the other three conclusions due to the errors in pressure and temperature calculation.

The above findings are derived from only one storm case at one analysis time. Further studies are needed using different sets of dual-Doppler data to study the kinetic energy budget of a convective storm at different stages of microburst development and with a different physical structure.

Acknowledgments. The authors wish to thank the National Center for Atmospheric Research for providing the dual-Doppler data and technical assistance. Thanks also go to R. G. Hughes and R. W. Pasken for their help in data reduction and computation. This material is based upon work supported by the Division of Atmospheric Sciences, National Science Foundation, under Grant ATM-8312172-01. John Coover was supported by the Air Force Institute of Technology.

REFERENCES

Fuelberg, H. E., and G. J. Jedlovec, 1982: A subsynoptic-scale kinetic energy analysis of the Red River Valley tornado outbreak (AVESESAME I). *Mon. Wea. Rev.*, **110,** 2005–2029.

——, and M. F. Printy, 1984: A kinetic energy analysis of the meso β-scale severe storm environment. *J. Atmos. Sci.*, **41,** 3212–3226.

Fujita, T. T., 1985: *The Downburst Microburst and Macroburst.* University of Chicago Press, 122 pp.

Gal-Chen, T., 1978: A method for the initialization of the anelastic equations: Implications for matching models with observations. *Mon. Wea. Rev.*, **106,** 587–606.

Hane, C. E., and P. S. Ray, 1985: Pressure and buoyancy fields derived from Doppler radar data in a tornadic thunderstorm. *J. Atmos. Sci.*, **42,** 18–35.

——, R. B. Wilhelmson and T. Gal-Chen, 1981: Retrieval of thermodynamic variables within deep convective clouds: Experiments in three dimensions. *Mon. Wea. Rev.*, **109,** 564–576.

Kessler, E., 1969: On the distribution and continuity of water substance in atmospheric circulations. *Meteor. Mongr.*, No. 32, Amer. Meteor. Soc., 84 pp.

Klemp, J. B., and R. B. Wilhelmson, 1978: The simulation of three-dimensional convective storm dynamics. *J. Atmos. Sci.*, **35,** 1070–1096.

Kung, E. C., and T. L. Tsui, 1975: Subsynoptic-scale kinetic energy balance in the storm area. *J. Atmos. Sci.*, **32,** 729–740.

Lin, Y. J., and R. G. Hughes, 1987: Structural features of a microburst-producing storm in Colorado revealed by JAWS dual-Doppler radars. *J. Atmos. Sci.*, **44,** 3640–3655.

——, T. C. Wang and J. H. Lin, 1986: Pressure and temperature perturbations within a squall-line thunderstorm derived from SESAME dual-Doppler data. *J. Atmos. Sci.*, **43,** 2302–2327.

——, R. G. Hughes and R. W. Pasken, 1987: Subcloud-layer kinematic and dynamic structures of a microburst-producing thunderstorm in Colorado determined from JAWS dual-Doppler measurements. *Bound-Layer Meteor.*, **39,** 67–86.

Srivastava, R. C., 1985: A simple model of evaporatively driven downdraft: Application to microburst downdraft. *J. Atmos. Sci.*, **42,** 1004–1023.

Tsui, T. L., and E. C. Kung, 1977: Subsynoptic-scale energy transformations in various severe storm situations. *J. Atmos. Sci.*, **34,** 98–110.

Wilson, J. W., R. D. Roberts, C. Kissinger and J. McCarthy, 1984: Microbursts wind structure and evaluation of Doppler radar for airport wind shear detection. *J. Climate Appl. Meteor.*, **23,** 898–915.